Electronic Supplementary Material (ESI) for Journal of Materials Chemistry A.


# Chemical Activated Hollow Carbon Nanospheres as a High-Performance Anode Material for Potassium Ion Batteries

Gang Wang[a], Xunhui Xiong[a,*], Dong Xie[b], Zhihua Lin[a], Jie Zheng[a], Fenghua Zheng[a], Youpeng Li[a], Yanzhen Liu[a], Chenghao Yang[a], Meilin Liu[c]

[a] Guangzhou Key Laboratory of Surface Chemistry of Energy Materials, New Energy Research Institute, School of Environment and Energy, South China University of Technology, Guangzhou 510006, China

[b] Guangdong Engineering and Technology Research Center for Advanced Nanomaterials, School of Environment and Civil Engineering, Dongguan University of Technology, Dongguan 523808, China

[c] School of Materials Science & Engineering, Georgia Institute of Technology, 771 Ferst Drive, Atlanta, GA 30332-0245, USA

* Corresponding Authors: esxxiong@scut.edu.cn (Xunhui Xiong)

**Experimental section**

**Material synthesis:** The HCSs were prepared by a routine self-template strategy. In a typical synthesis process, 3 mL of ammonia hydroxide (25 wt %) was dispersed into a mixed solution of water and ethanol with a volume ratio of 1:7 under vigorous magnetic stirring. Afterwards, 0.01 mol tetraethylorthosilicate (TEOS) was drop-wise added into the hydroalcoholic solution. After 30 min, formaldehyde solution (0.56 mL, 37 wt %) and resorcinol (0.4 g) were added into above mixed solution, and stirred for 24 h at 25 °C. The obtained precipitate was collected by centrifuging and washing with deionized water and absolute ethanol for several times, and then the dried powders (60 °C for 12 h) was thermally treated for 2 h at 800 °C under Ar gas flow in a tube furnace. The HCSs were obtained by removing silica using hydrofluoric acid solutions (10 wt %). Finally, the HCSs were dispersed in 6 M KOH solution under stirring for 4 h and then submerged for another 20 h at room temperature. To investigate the effect of synthetic parameters on materials properties, the KOH activation process at 12 h and 36 h was also prepared. After filtration and drying, the AHCSs undergo heat treatment at 800 °C for 1 h under an Ar flow with a rate of 5 °C $min^{-1}$.

**Materials characterization:** The field-emission scanning electron microscope (FE-SEM, Hitachi SU8010) and transmission electron microscopy (TEM, Tecnai G2 F20 S-TWIN) were used to observe the morphology of the as-prepared materials. The microstructure of the as-prepared material was characterized by powder X-ray diffraction (XRD, Bruker D8 Advance, Cu Kα radiation at λ=1.54178 Å) and Raman microscopy (Renishaw RM1000). Brunauer-Emmett-Teller (BET) surface area and

Barrett-Joyner-Halenda (BJH) pore distribution were obtained on a ASAP 2020 HD88 (Micromeritics) sorption analyzer.

**Electrochemical measurements:** Electrochemical tests were carried out in 2032 coin-type cells. The anode electrode was prepared by mixing the active material, acetylene black, and polyvinylidene fluoride (PVDF) binder with a mass ratio of 8:1:1 in N-methyl-2-pyrrolidone solvent. The obtained slurry was coated onto copper (Cu) foil and dried at 110 °C under vacuum for 12 h. Generally, the mass loading of the HCSs and AHCSs cathode material is about 0.2 mg $cm^{-2}$. Potassium metal anode was served as both the counter and reference electrode. The electrolyte was 0.8 mol $L^{-1}$ $KPF_6$ in a mixture of ethylene carbonate (EC) and diethyl carbonate (DEC) (1:1 in volume ratio), and the separator was glass fiber paper. The coin cells were assembled in an argon-filled glove box with water and oxygen concentrations below 0.1 ppm. Galvanostatic measurements were monitored using a LAND CT2001A battery-testing system at ambient temperature, where the voltage range was from 0.01 to 3 V *vs* $K^+/K$. Cyclic voltammeter (CV) and Electrochemical impedance spectroscopy (EIS) tests were recorded on an electrochemical workstation (CHI660a, Shanghai Chenhua).

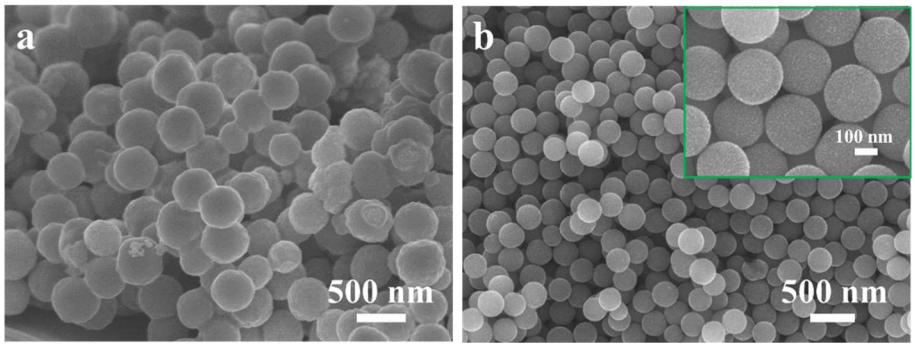


**Fig. S1** SEM images of (a) the RF/$SiO_2$ nanospheres and (b) the C/$SiO_2$ nanospheres.

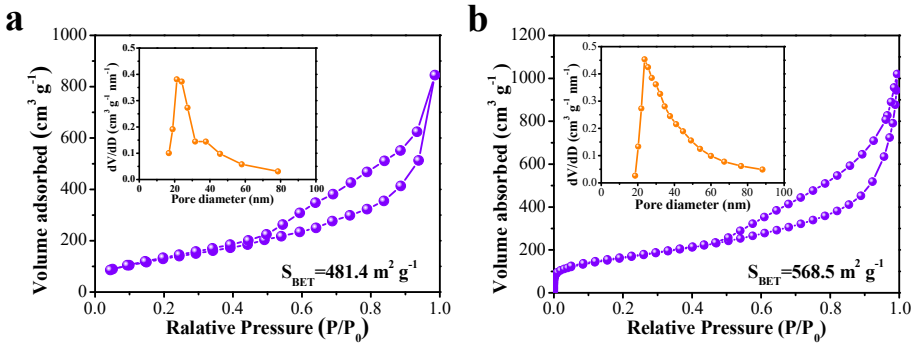


**Fig. S2** $N_2$ adsorption/desorption isotherm of (a) HCSs and (b) AHCSs activated for 12 h, insert is the corresponding pore size distribution.

After chemical activation, the BET specific surface area was increased from 481.4 to 568.5 and 757.8 $m^2$ $g^{-1}$. The type-IV isotherm with pronounced hysteresis indicates the existence of a large number of mesopores. Meanwhile, the pore volume of AHCSs was also improved. The enhanced specific surface area and pore volume not only boost the transfer of electron/$K^+$, but also alleviate the volume change during cycling.

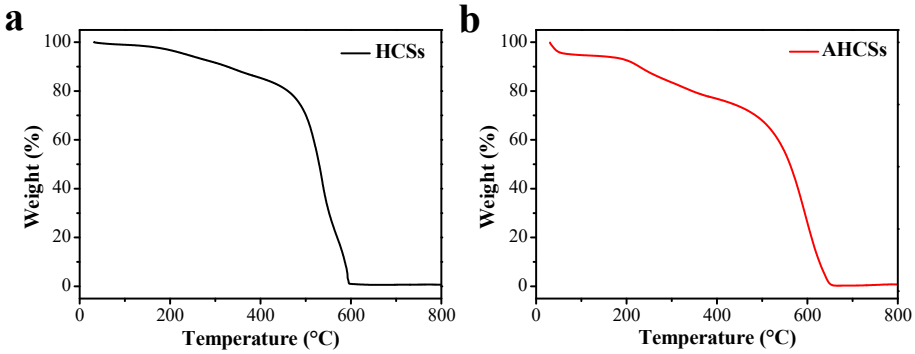


**Fig. S3** TG curves of the HCSs and AHCSs samples.

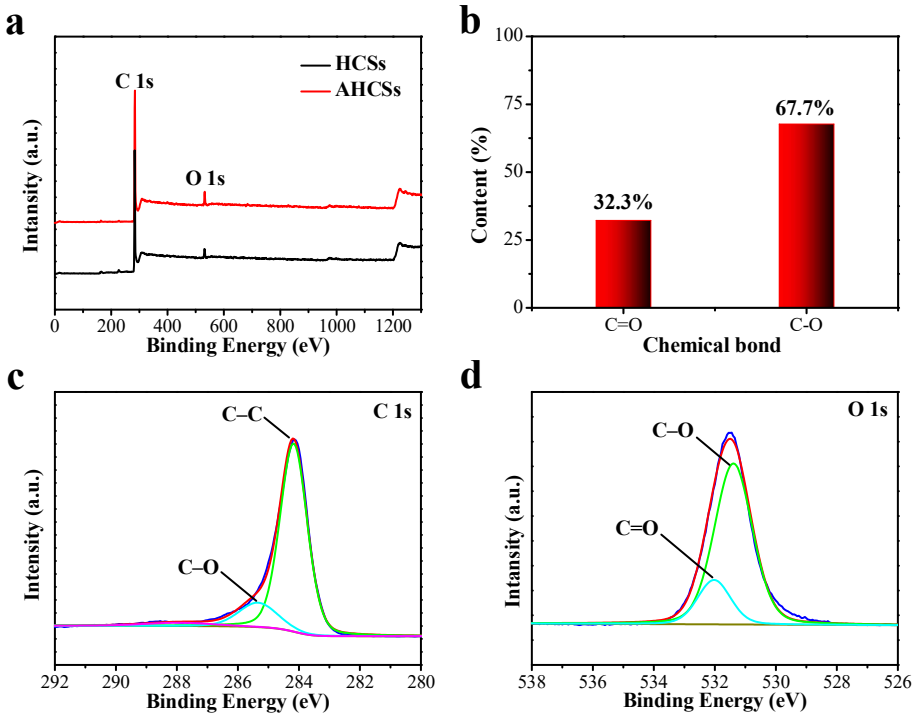


**Fig. S4** (a) Survey XPS spectra of the HCSs and AHCSs, (b) the percentage of C=O and C–O for AHCSs, High-resolution XPS spectra of (c) C 1s and (d) O 1s of HCSs.

**Table 1** Atomic content of C and O for HCSs and AHCSs.

| Sample | Atomic content (%) | |
|---|---|---|
| | C | O |
| HCSs | 97.92 | 2.08 |
| AHCSs | 95.54 | 4.46 |

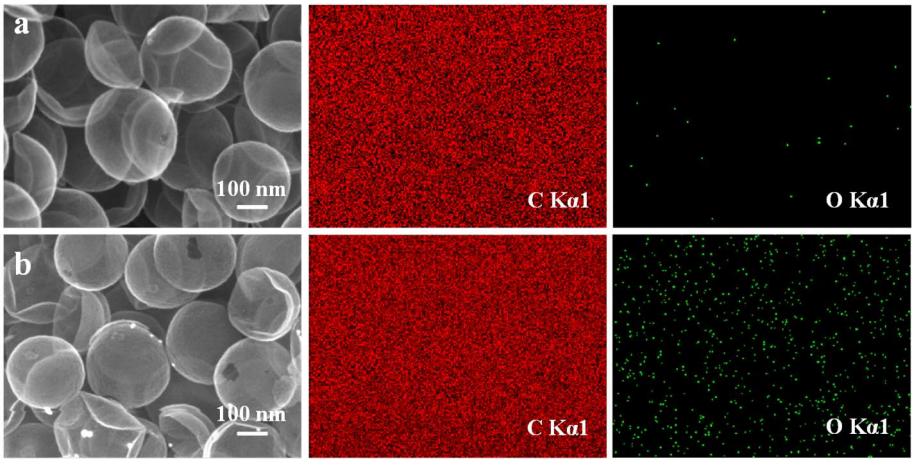


**Fig. S5** SEM image and corresponding EDS mapping (C, O) of (a) the HCSs and (b) AHCSs.

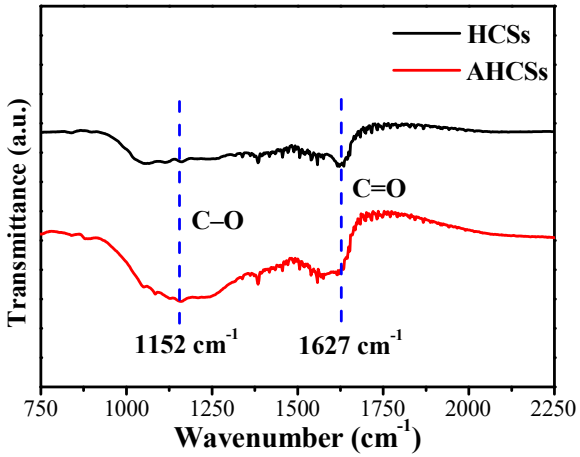


**Fig. S6** FT-IR spectrum of the HCS and AHCSs.

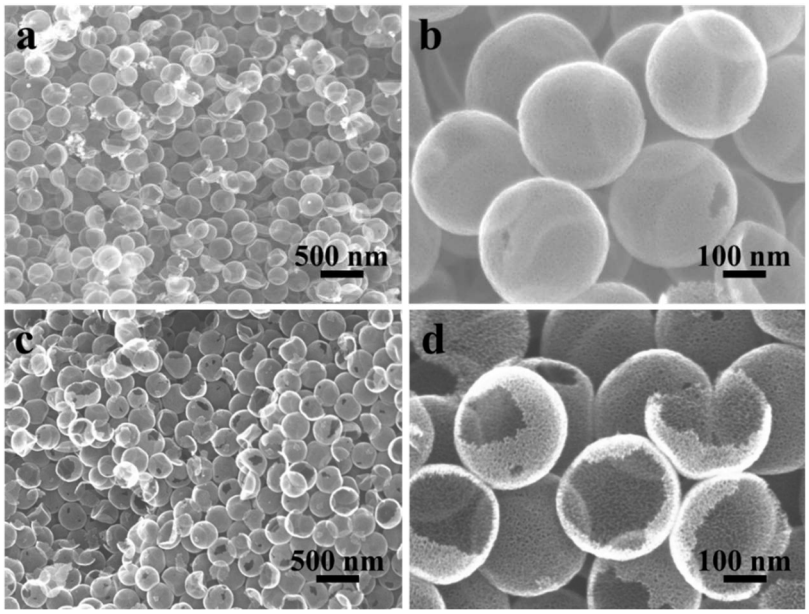


**Fig. S7** SEM images of AHCSs after KOH for (a,b) 12 h and (c,d) 36 h.

Fig. S7 shows the morphologies of samples that activated for 12 h and 36 h followed by high temperature calcination (800 °C for 1 h), respectively. After activated for 12 h, despite the spherical texture of the AHCSs was preserved essentially, the BET specific surface area and pore volume increased less (Fig. S2b). When the activation time was extended to 36 h, the spherical structure was collapsed (Fig. S7c and S7d).

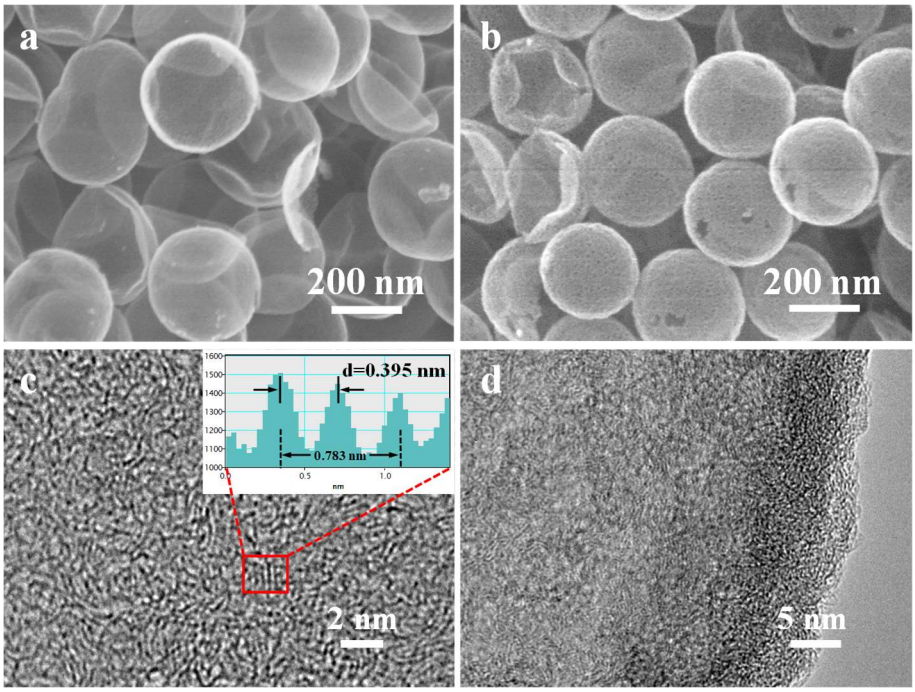


**Fig. S8** SEM image of the (a) HCSs and (b) AHCSs at high magnification, HRTEM images of (c) HCSs and (d) AHCSs.

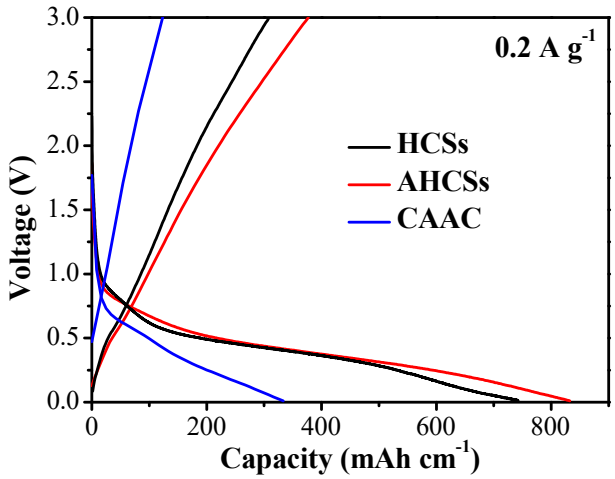


**Fig. S9** The initial charge/discharge curves of the HCSs, AHCSs and commercial

available activated carbon (CAAC).

The HCSs electrode delivers an initial charge and discharge specific capacity of 306.7 and 742.2 mAh $g^{-1}$ at 0.2 A $g^{-1}$ with a Coulombic efficiency of 41.3%, while the CAAC exhibits a low charge and discharge capacity of 123.1 and 333.5 with a low Coulombic efficiency 36.9%.

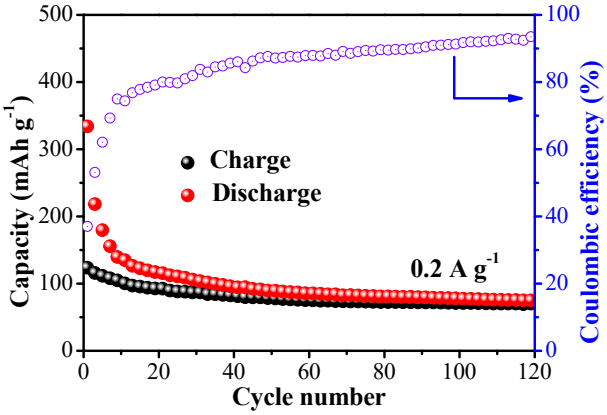


**Fig. S10** Cycle performance of commercial available activated carbon at 0.2 A $g^{-1}$.

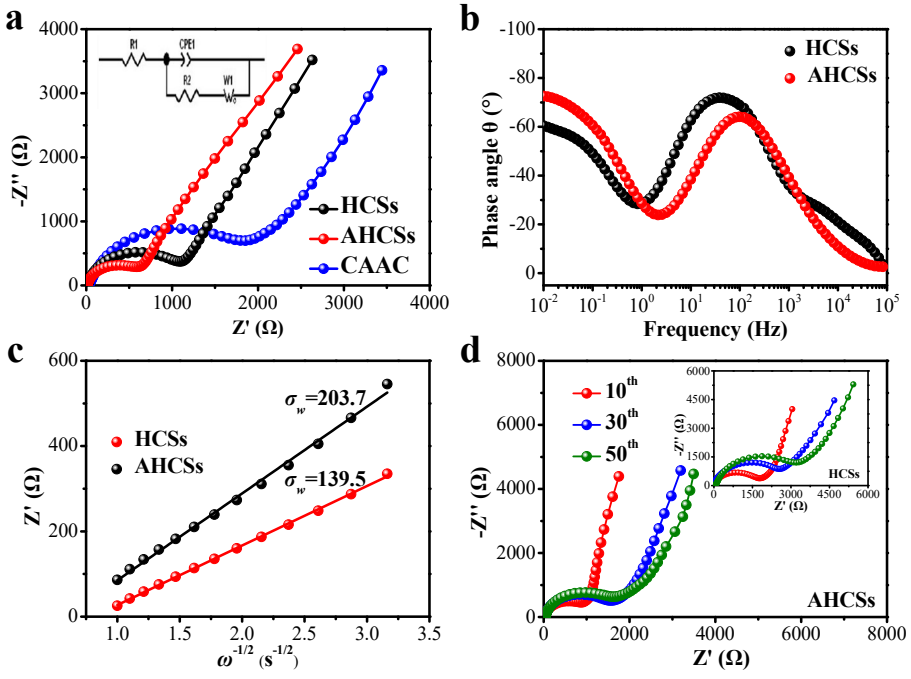


**Fig. S11** (a) EIS spectra and (b) corresponding Bode diagrams for the HCSs and AHCSs electrodes, (c) the linear relationship of Z' *vs.* $\omega^{-1/2}$ at low frequency region of HCSs and AHCSs electrodes, (d) EIS spectra of AHCS electrode at different cycles after fully

charging to 3 V. The inset shows the spectra of HCS electrode.

**Table 2** The simulated results from electrochemical impedance spectra of HCSs and AHCSs samples.

| Sample | Cycle | $R_s$ (Ω) | $R_{ct}$ (Ω) | $W_o$ (Ω) | $D_{K^+}$ ($cm^{-2}$ $s^{-1}$) |
|---|---|---|---|---|---|
| HCSs | 1st | 7.11 | 994.6 | 1754.3 | $2.04\times10^{-15}$ |
| | 10th | 10.15 | 1613.7 | 2876.0 | |
| | 30th | 12.02 | 2279.7 | 4105.8 | |
| | 50th | 14.26 | 2874.4 | 4467.9 | |
| AHCSs | 1st | 6.03 | 580.7 | 1160.5 | $6.85\times10^{-15}$ |
| | 10th | 8.75 | 819.9 | 1543.2 | |
| | 30th | 9.94 | 1429.0 | 2751.6 | |
| | 50th | 12.65 | 1446.2 | 2786.1 | |

To get insight into the electrochemical reaction process, EIS of the HCSs and AHCSs electrodes at different cycles were measured and presented in Fig. S10. All the Nyquist plots are consisted of a semicircle at high frequency and a slope line at low frequency, where the semicircle is ascribed to the charge transfer resistance ($R_{ct}$) and the slope line region is related to the K ion diffusion process. The simulated electrochemical parameters are shown Table. Obviously, the $R_{ct}$ value of AHCSs is much less than that of HCSs, implying the enhancement of the reaction kinetics for AHCSs electrode. From the corresponding Bode plot (Fig. S10b), it can be observed that the phase angle in the low frequency region was decreased for AHCSs electrode, demonstrating an improved diffusion of $K^+$.[1,2] The $K^+$ ion diffusion coefficient ($D_{K^+}$) of HCSs and AHCSs electrodes can be calculated according to the following

equations:[3-5]

$$D_{K^+} = \frac{R^2T^2}{2A^2n^4F^4C^2\sigma_w^2} \quad (1)$$

where $R$ is the gas constant, $T$ is the absolute temperature, $A$ is the surface area of the cathode, $n$ is the number of electrons per molecule during oxidization, $F$ is the Faraday constant, $C$ is the concentration of $K^+$ ion, $\sigma_w$ is the Warburg factor which is relative with Z'.

$$Z' = R_s + R_{ct} + \sigma_w\omega^{-1/2} \quad (2)$$

$R_s$ is the resistance of the electrolyte and electrode material, $R_{ct}$ is the charge transfer resistance and $\omega$ is the angular frequency in the low frequency region.

During the cycling, the $R_{ct}$ value of the HCSs electrode increased greatly from the 1st to the 50th. By contrast, the $R_{ct}$ value of the 50th for AHCSs electrode is quite close to that of the 30th, indicating that the oxygen-containing functional groups on AHCSs surface facilitate the formation of stable SEI film. Similarly, the Warburg diffusion impedance ($W_o$) of the AHCSs electrode is lower than that of the HCSs electrode, demonstrating that the excellent rate capability can be related to the improvement of K ions diffusion originated from the enlarged interlayer space and introduced oxygen-containing functional groups.

**Table 3** Compared the cyclic stability of the as-prepared AHCSs with other carbon-based materials in KIBs.

| Materials | Current density ($A\ g^{-1}$) | Cycle number | Cycled capacity ($mAh\ g^{-1}$) | References |
|---|---|---|---|---|
| N-doped graphene | 0.1 | 100 | 210 | Ref.6 |
| Activated carbon | 0.2 | 100 | 100.3 | Ref.7 |
| Expanded graphite | 0.2 | 500 | 174 | Ref.8 |
| Porous carbon nanofiber | 0.2 | 1200 | 211 | Ref.9 |
| Short-range order carbon | 1 | 1000 | 146.5 | Ref.10 |
| N-doped carbon nanofiber | 1 | 1000 | 203.1 | Ref.11 |
| S/O-doped carbon | 1 | 2000 | 108.4 | Ref.12 |
| N-doped porous carbon | 1 | 3000 | 152 | Ref.13 |
| N-doped carbon nanotube | 2 | 500 | 102 | Ref.14 |
| CAAC | 0.2 | 120 | 70.1 | |
| HCSs | 2 | 5000 | 109.8 | This work |
| AHCSs | 2 | 5000 | 192.7 | |

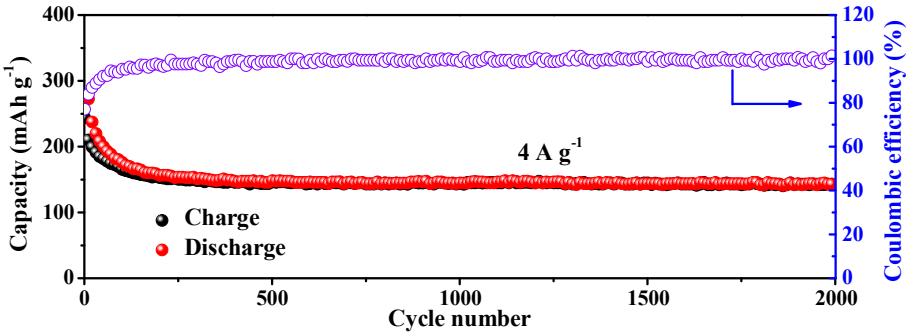


**Fig. S12** High-rate cycle performance of the AHCSs at a 4.0 A $g^{-1}$.

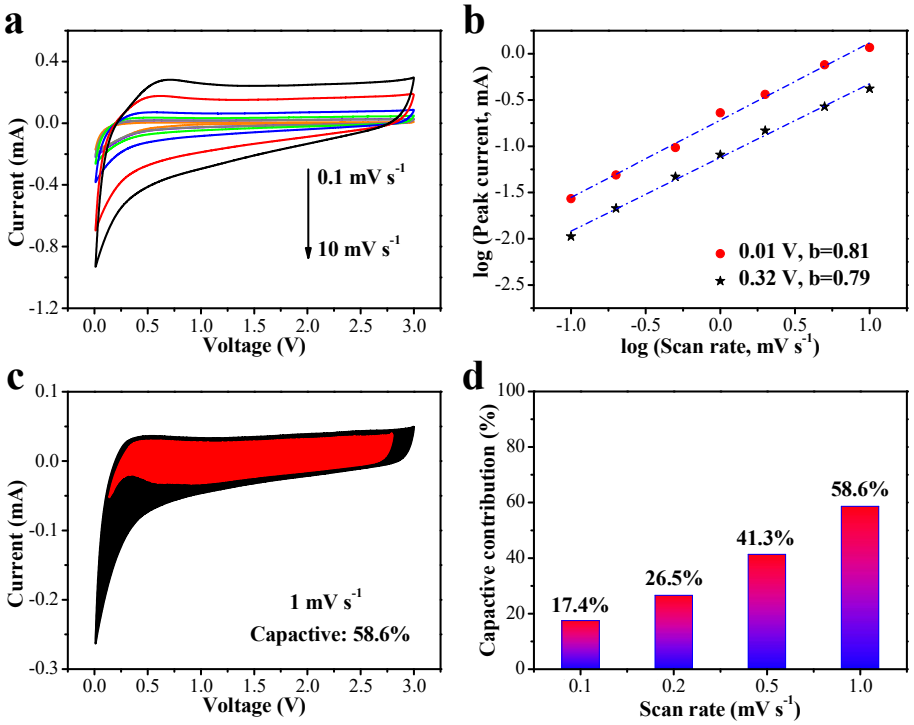


**Fig. S13**. (a) CV profiles of HCSs at various scan rates from 0.1 to 10 mV $s^{-1}$. (b) Measurement of the *b* value with linear the relationship between log*i* and log*v*. (c) Capacitive contribution of HCSs to total charge storage at 1 mV $s^{-1}$. (d) Normalized contribution ratio of capacitive capacities for HCSs at various scan rates.

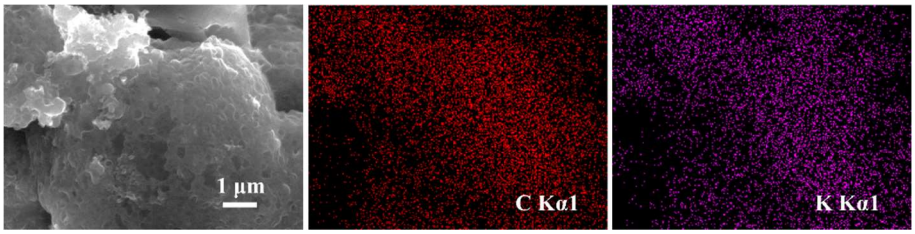


**Fig. S14** SEM and corresponding EDS mapping of C and K in AHCSs electrode at full potassiation state.

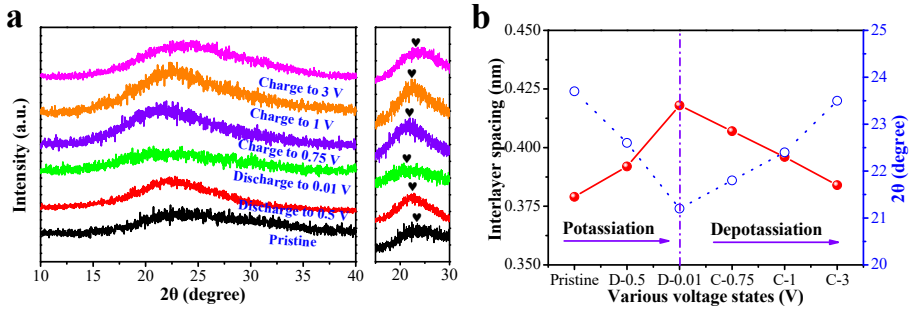

**Fig. S15** (a) *Ex*-XRD and (b) the interlayer spacing and corresponding peak location at various stages of HCSs.

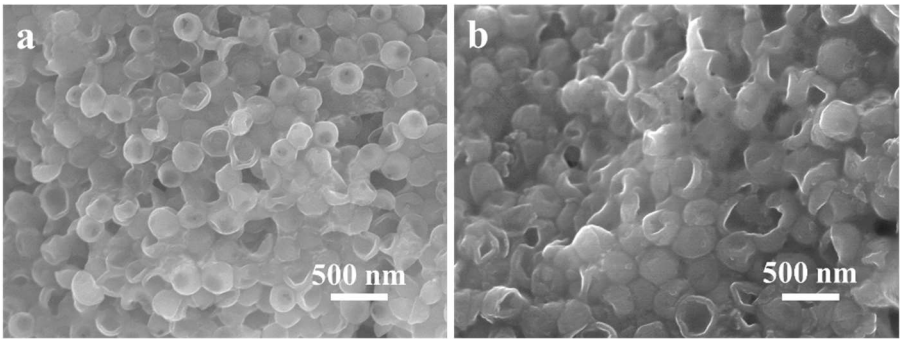


**Fig. S16** SEM images of the AHCSs electrode after (a) 2000 and (b) 5000 cycles at a current density of 2 A $g^{-1}$.

## References


[1] Y. Oumellal, N. Delpuech, D. Mazouzi, N. Dupré, J. Gaubicher, P. Moreau, P. Soudan, B. Lestriez and D. Guyomard, *J. Mater. Chem*., 2011, **21**, 6201-6208.

[2] A. Ponrouch, A. R. Goñi and M. Rosa Palacín, *Electrochem. Commun.*, 2013, **27**, 85-88.

[3] L. Yi, X. Wang, G. Wang, Y. Bai, M. Liu, X. Wang and R. Yu, *Electrochim. Acta*, 2016, **222**, 1354-1364.

[4] X. Ou, X. Liang, C. Yang, H. Dai, F. Zheng, P. Wu, Q. Pan, X. Xiong and M. Liu, *Energy Storage Materials*, 2018, **12**, 153-160.

[5] Y. Liu, C. Yang, Q. Pan Y. Li, G. Wang, X. Ou, F. Zheng, X. Xiong, M. Liu and Q. Zhang, *J. Mater. Chem. A*, 2018, **6**, 15162-15169.

[6] K. Share, A. P. Cohn, R. Carter, B. Rogers and C. L. Pint, *ACS Nano*, 2016, **10**, 9738-9744.

[7] Z. Tai, Q. Zhang, Y. Liu, H. Liu and S. Dou, *Carbon*, 2017, **123**, 54-61.

[8] Y. An, H. Fei, G. Zeng, L. Ci, B. Xi, S. Xiong and J. Feng, *J. Power Sources*, 2018, **378**, 66-72.

[9] X. Zhao, P. Xiong, J. Meng, Y. Liang, J. Wang and Y. Xu, *J. Mater. Chem. A*, 2017, **5**, 19237-19244.

[10] W. Wang, J. Zhou, Z. Wang, L. Zhao, P. Li, Y. Yang, C. Yang, H. Huang and S. Guo, *Adv. Energy Mater.*, 2018, **8**, 1701648.

[11] H. Zhu, C. Wang, C. Li, L. Guan, H. Pan, M. Yan and Y. Jian, *Carbon*, 2018, **130**, 145-152.

[12] M. Chen, W. Wang, X. Liang, S. Gong, J. Liu, Q. Wang, S. Guo and H. Yang, *Adv. Energy Mater*., 2018, **8**, 1800171.

[13] Y. Xie, Y. Chen, L. Liu, P. Tao, M. Fan, N. Xu, X. Shen and C. Yan, *Adv. Mater*., 2017, **29**, 1702268.

[14] P. Xiong, X. Zhao and Y. Xu, *ChemSusChem*, 2018, **11**, 202-208.